The International Journal of Advanced Manufacturing Technology (2026) 145:8907–8924
https://doi.org/10.1007/s00170-026-18809-9

ORIGINAL ARTICLE

Influence of top-surface condition and process parameters on cutting forces and surface integrity in CFRP milling

Levente Bukor[1] · Rao Fu[2,3] · Norbert Geier[1]

Received: 11 March 2026 / Accepted: 20 July 2026 / Published online: 28 July 2026

Abstract

The machinability of unidirectional carbon-fibre reinforced polymer (UD-CFRP) composites is strongly dependent on fibre architecture, cutting parameters and the initial surface condition; however, their combined effects remain insufficiently quantified. This study systematically evaluates the influence of fibre orientation (0°, 45°, 90°, 135°), feed (0.05 and 0.15 mm), cutting depth (1 and 2 mm) and top-surface quality (pre-machined by machining vs. abrasive water jet machining (AWJM)) on cutting forces and surface integrity during dry face milling. UD-CFRP composites were up-milled using a Ø12 mm Alcrona-coated two-flute carbide endmill. Three-component cutting force was recorded with a Kistler 9257B dynamometer and processed using a Butterworth low-pass filter. Surface roughness was measured in accordance with ISO 4288:1996, and surface morphology was assessed by optical and scanning electron microscopy. ANOVA results identify cutting depth and feed as the primary drivers of resultant cutting force, while the initial top-surface condition was also found to be significant. Fibre orientation did not significantly affect force in the pooled dataset, but became significant for pre-machined specimens, indicating that consistent allowance is required to reveal orientation effects. Surface roughness was strongly dependent on fibre orientation — optimal finishes were observed at 0° and 90°, whereas 135° produced the poorest results. SEM analysis revealed extensive matrix smearing that can obscure subsurface defects (fibre pull-out, microcracks), potentially biasing profilometric measurements. The results support the need for pre-machining of AWJ-cut CFRP specimens to improve repeatability and consistency, and recommend that fibre orientation and subsurface inspection be considered when specifying machining strategies for CFRPs.

Keywords CFRP · Machining · Cutting force · Surface roughness · SEM

1 Introduction

Carbon fibre-reinforced polymer (CFRP) composites are increasingly used across high-end industrial applications (e.g., wind-turbine blades [1], aircraft fuselages [2]) and consumer products (e.g., drones [3], sports equipment [4]). Generally, the structural integrity of these composites is highly sensitive to their specific manufacturing conditions and thermal environments [5, 6]. The wider use of CFRPs makes the optimisation of manufacturing processes increasingly important so that strict geometric tolerances can be met while production cost and material damage are minimised [7]. In many CFRP components, holes and edges are finished by mechanical machining [8–12]; therefore, a detailed understanding and technological development of CFRP machining are essential.

To characterise chip-formation mechanisms and to develop predictive models (such as numerical simulations, digital twins, and process-monitoring algorithms), researchers commonly perform orthogonal cutting experiments on CFRP at different fibre cutting angles [13–15]. By testing the full range of orientations (0°–180°) that occur in realistic drilling and milling technologies, angle-dependent cutting

✉ Norbert Geier
geier.norbert@gpk.bme.hu

[1] Department of Manufacturing Science and Engineering, Faculty of Mechanical Engineering, Budapest University of Technology and Economics, Műegyetem rkp. 3., Budapest 1111, Hungary

[2] State Key Laboratory of High-Performance Precision Manufacturing, School of Mechanical Engineering, Dalian University of Technology, Dalian 116024, China

[3] Key Laboratory of High-Performance Manufacturing for Advanced Composite Materials, Dalian 116024, Liaoning Province, China

responses can be measured and then superposed to predict the mechanics and energetics of more complex operations [16–19]. Wang and Zhang [20] highlighted the characteristic phenomenon of 'bouncing back' in CFRP machining, where the elastic recovery of the composite fibres against the tool flank face significantly influences thrust forces and dimensional accuracy. They identified that when $\theta < 90°$, material removal is characterised by chipping and pressing. However, when $\theta > 90°$, the mechanism shifts to fibre bending and crushing, leading to severe subsurface damage. This was corroborated by Wang et al. [21], who investigated surface cavity defects in milling, confirming that the most severe defects occur at around 135° of fibre cutting angle due to fibre-matrix interface debonding. An et al. [13] further classified these mechanisms, noting that parallel cutting ($\theta = 0°$) relies on interface layering separation dominated by in-plane shear stress, yielding the smoothest surfaces. Conversely, perpendicular cutting ($\theta = 90°$) involves shear-fracture separation, which requires higher specific cutting energies. Karpat et al. [22] proposed a mechanistic cutting force model for milling unidirectional CFRPs. They identified distinct chip formation modes: peeling at $\theta = 0°$ and compressive shear failure at $\theta = 90°$. Qi et al. [23] developed a force prediction model based on the Minimum Potential Energy Principle. Their work analysed the deflection of a single fibre (Representative Volume Element) and predicted the critical force required for fracture, effectively modelling slipping, peeling, and bounding mechanisms across different orientation sectors.

These findings were supported by further orthogonal cutting experiments [24, 25], which confirmed that specific cutting forces decrease with increasing chip thickness — a 'size effect' analogous to metal cutting [26, 27]. Notably, advanced strategies have been introduced to overcome the limitations of conventional cutting; for instance, Zhang et al. [28] utilised ultrasonic vibration-assisted (UVA) cutting to alter chip formation from continuous crushing to discrete fracture events, while Shu et al. [2] developed a dedicated drill bit geometry that shifts the mechanism from compression to shear cutting, both successfully reducing cutting forces and thermal loads.

A critical distinction must be made between surface delamination and subsurface damage. Hintze et al. [29] identified the $90° < \theta < 180°$ range as critical for delamination due to the lack of support for top plies. While this range is prone to surface defects, Böhland et al. [30] highlighted that the theoretically 'safe' 0–90° range is susceptible to severe subsurface damage (interlaminar cracks) due to compressive bending. To accurately predict these risk areas, Li et al. [31] proposed the 'Cutting Geometry Space' (CGS), a 3D framework that decouples cutting, feeding, and fibre tilt angles to identify specific 'Damage Zones'. Geier and Pereszlai [32] demonstrated that the R_z/R_a ratio is a far more sensitive indicator than R_a alone for detecting characteristic CFRP defects like fibre pull-outs.

Turki et al. [33] highlight the correlation between orthogonal cutting and drilling. They demonstrated that defects in orthogonal cutting at $90° < \theta < 180°$ directly correspond to hole-exit delamination in drilling. This 'against-fibre' cutting mode generates axial thrust forces that push plies apart. Additionally, the optimization of stacking sequences and the use of proper back-up supports have been shown to critically influence and mitigate such drilling-induced delamination [34–38]. Li et al. [39] provided a crucial industrial strategy by investigating damage behaviours in multiple-pass cutting. Unlike academic single-pass studies, they showed that a preliminary pass relieves stress concentrations for subsequent cuts. Their multiple-pass strategy reduced fibre breakage length by 40% and pull-out depth by 63% compared to single-pass cutting, offering a practical method to enhance surface quality without changing tool materials.

Although orthogonal cutting tests yield essential information for physical understanding and model calibration, there is no widely adopted open standard describing how these experiments should be conducted. As a result, reproducibility and comparability across studies are often limited. A major practical challenge —especially for thin composite plates— is the preparation of the surface that will be orthogonally machined (the surface where the nominal chip thickness is realised). Different preparation techniques can change the local topography, fibre exposure and edge condition, all of which strongly affect measured cutting forces, chip formation and surface finish. Han et al. [40] implemented a rigorous specimen preparation protocol wherein the UD-CFRP substrates were pre-machined to eliminate initial surface irregularities, followed by the application and subsequent precision turning of the epoxy coating to a controlled thickness. This procedure was designed to ensure uniform experimental conditions and to isolate the coating's restraining effect, thereby accurately evaluating its efficacy in mediating the compositional machining difference between the carbon fibres and the polymer matrix. Vallejo et al. [41] employed CNC face and peripheral milling to prepare the surfaces of 3D-printed carbon fibre-reinforced composites, concluding that although this machining process significantly reduced surface roughness, the presence of fibre reinforcement led to severe surface tearing during peripheral milling. Qin et al. [42] reported that before each orthogonal cutting test, the workpiece's top was machined flat to eliminate any non-parallel misalignment between the surface and cutting direction, thereby guaranteeing a consistent chip thickness during the experiment. This preparatory planning or face-milling step helps standardise the chip load across all trials.

Abrasive water jet machining (AWJM) and conventional mechanical machining are two methods frequently used to prepare the top surface of specimens for orthogonal cutting. However, the influence of these preparation techniques on experimental reproducibility and on the measured cutting response has received limited systematic attention. The present experimental study addresses this gap by directly comparing AWJM and the mechanical preparation of CFRP top surfaces. We quantified how cutting force and resulting surface characteristics depend on fibre orientation for specimens prepared by each method, and we evaluated which preparation procedure yields a consistent, well-defined chip thickness suitable for reproducible machining tests like orthogonal cutting.

Specifically, this work (i) compares AWJM and mechanically prepared top surfaces across the full range of fibre orientation angles, (ii) assesses the resulting cutting-force signals and surface quality metrics, and (iii) demonstrates that mechanically machined specimens —prepared by a flat-surface milling protocol— provide a reproducible nominal chip thickness and more consistent cutting outcomes. By clarifying the role of specimen-topology preparation, our results aim to improve the comparability of machining experiments (e.g., edge trimming, orthogonal cutting) and to provide practical guidance for future experimental and modelling studies of CFRP machining. Furthermore, since recent studies have demonstrated that tool-workpiece interaction and cutting configurations significantly alter the force profiles and resulting surface morphology [43], standardizing the initial surface condition is increasingly vital.

2 Experimental setups

A hand lay-up laminated epoxy resin-based unidirectional CFRP composite was used. The composite laminate was produced using MR3124 epoxy resin with a FM20 hardener in a ratio of 175 g per 500 g of resin. Unidirectional reinforcement was achieved by carefully aligning the carbon fibre fabric during lay-up. After lamination, the workpiece was placed between two glass plates and loaded with a total weight of 100 kg for 24 h to ensure consolidation and proper resin distribution. Following this pressing stage, the laminate underwent a post-cure heat treatment in an oven at 60 °C for 4 h to enhance the mechanical properties and stability of the composite. The key material properties of the composite were measured and summarised in Table 1.

Table 2 Process parameters for abrasive water jet cutting, where p denotes the pressure and v is the speed of the nozzle

Dimensions (mm)	p (bar)	v (mm/min)	Abrasive material
15 × 30	3600	460	80-mesh granite sand

The UD-CFRP specimens were sectioned into 8 pieces, having 15 × 30 mm dimensions using a Perndorfer WSS 4020 water jet cutting system. The process parameters shown in Table 2.

The milling experiments were conducted on a Kondia B640 CNC 3-axis machining centre (Fig. 1a). The composite chips and dust were removed with a Nilfisk GB733 industrial vacuum cleaner. During the milling process, coolant lubricant was not used (i.e., experiments were conducted under dry conditions). A solid carbide, Alcrona-coated Tivoly P652 end mill was used, having two cutting edges and a nominal diameter of Ø 12 mm, as shown in Fig. 1a and illustrated in Fig. 1b and c. The UD-CFRP was fixed in a clamp on the dynamometer. The sides of UD-CFRP composites were pre-machined (contour milled) with the same cutting tool, after it was fixed into the clamp and before the experiments, to ensure a constant width of cut (a_e) for the experiments.

Full factorial machining experiments were conducted at four levels of fibre orientation (0°, 45°, 90°, 135°), two levels of feed (0.05 mm, 0.15 mm), cutting depth (1 mm, 2 mm) and quality of the top of the composite (raw, i.e., prepared by AWJM; and pre-machined by milling) as shown in Table 3. The process parameters were selected based on the tool manufacturer's recommended cutting conditions for finishing applications. The interpretation of the factor of the quality of the top of the composite is illustrated in Fig. 1c. The fixed values were as follows: cutting speed (v_c) of 100 m/min, width of cut (a_e) of 6 mm, and the milling technology was up-milling (also known as conventional milling). Tool wear was considered negligible and therefore excluded from the investigation, as the total cumulative cutting length of approximately 480 mm represented only 10% of the expected tool life.

Cutting force was measured with a KISTLER 9257B three-component dynamometer. The signal was amplified using a KISTLER 5070 multi-channel charge amplifier, and the data was collected by two National Instruments USB-4431 dynamic signal acquisition modules and a LabVIEW program. The measurement sampling frequency was 3 500 Hz (i.e., force data was collected at every 5° spin of the cutting tool and the signal also included higher-order

Table 1 Key material properties of the applied CFRP composite [44], where σ denotes the tensile strength, C is the impact strength, τ is the interlaminar shear strength, S_D is the Shore D hardness, w_f is the fibre weight fraction, N_p is the ply number, h_{ply} is the ply thickness and $s*$ denotes the standard deviation of measured data

$\sigma \pm s*$ (MPa)	$C \pm s*$ (kJ/m^2)	$\tau \pm s*$ (MPa)	$S_D \pm s*$ (1)	w_f (%)	N_p (1)	h_{ply} (mm)
723.00 ± 58.29	194.07 ± 31.57	19.26 ± 0.76	85.5 ± 1.9	45.65	27	0.5 − 0.6

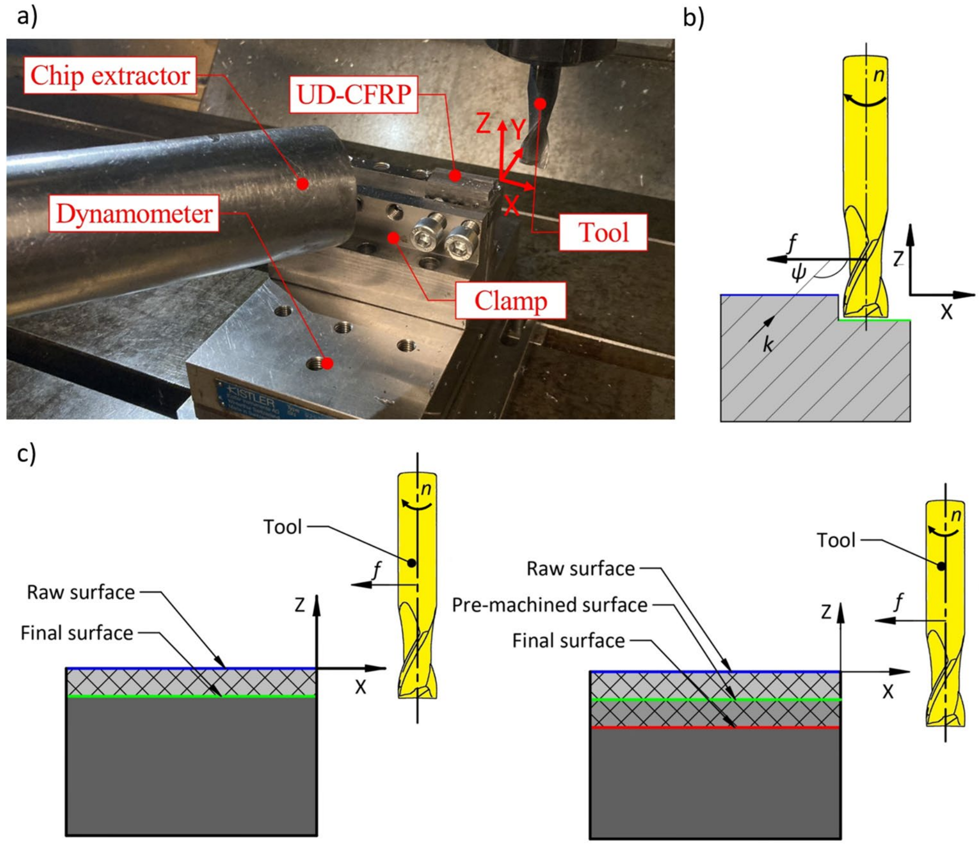

Fig. 1 Illustration of the **a**) experimental setup, **b**) schematic drawing of the interpretation of the fibre orientation (ψ), **c**) schematic drawing of the interpretation of the quality of the top of the composite (Q), where the "Raw surface" is prepared by AWJM technology, k denotes the fibre direction, n is the spindle speed, and f is the feed

Table 3 Experimental factors and their levels

Factor		Levels			
		1	2	3	4
Fibre orientation (°)	ψ	0	45	90	135
Cutting depth (mm)	a_p	1	2		
Feed (mm)	f	0.05	0.15		
Quality of the top of the composite (1)	Q	Q_1: raw	Q_2: pre-machined		

harmonics). The cutting force components were processed in a MATLAB code. The cutting force components were first transformed by fast Fourier transformation (FFT), then filtered with a Butterworth low-pass filter (chosen for its gradual roll-off characteristic that preserves force peaks) using a cut-off frequency of 500 Hz (five times the 86.7 Hz fundamental tooth passing frequency with a safety margin), as shown in Fig. 2. The filtered data are expressed by

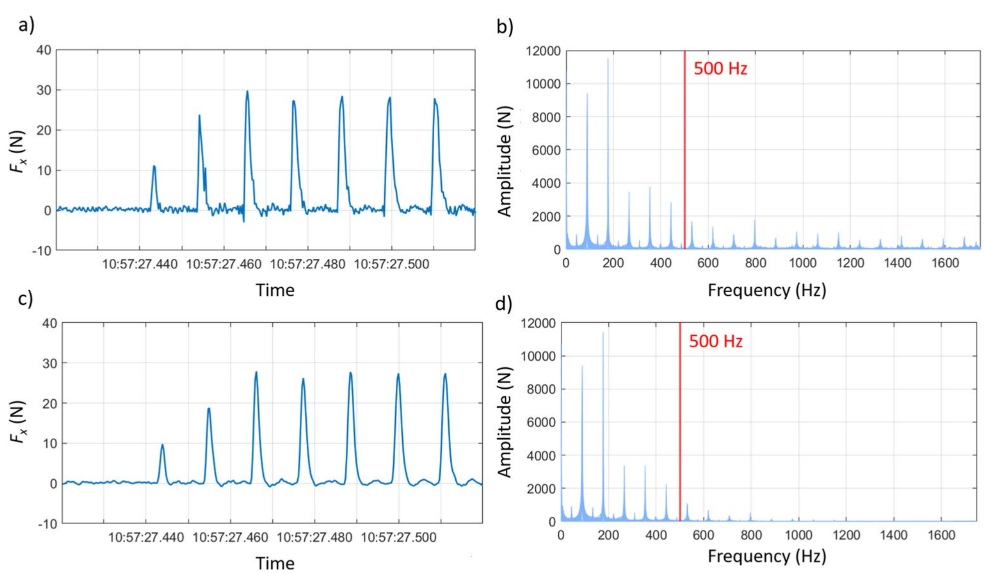

Fig. 2 Representative graphs illustrating the filtering of the F_x cutting force component: **a**) unfiltered F_x, **b**) frequency-amplitude diagram of the unfiltered F_x, **c**) filtered F_x, **d**) frequency-amplitude diagram of the filtered F_x

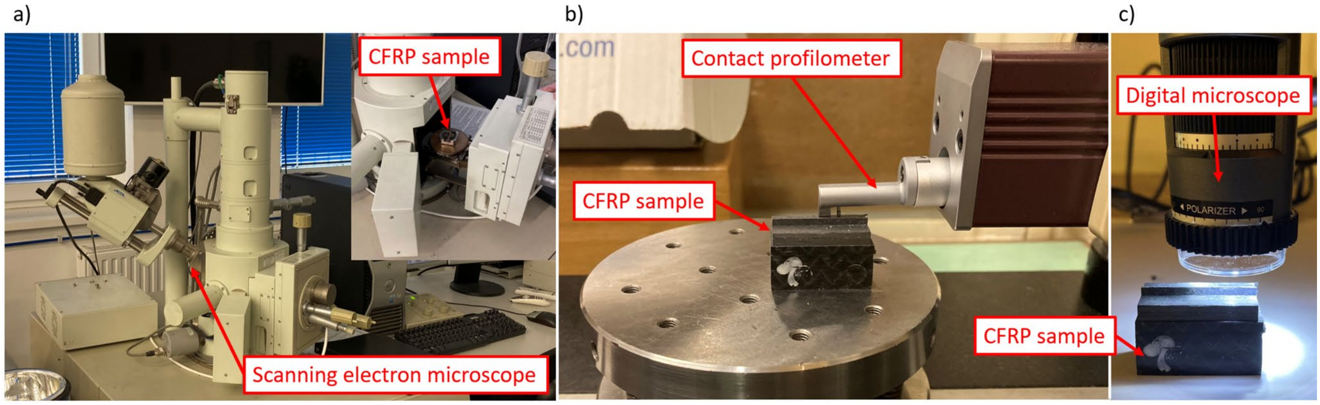

Fig. 3 Applied measuring devices: **a**) Jeol SEM, **b**) Mitutoyo contact profilometer, and **c**) Dino-Lite digital microscope

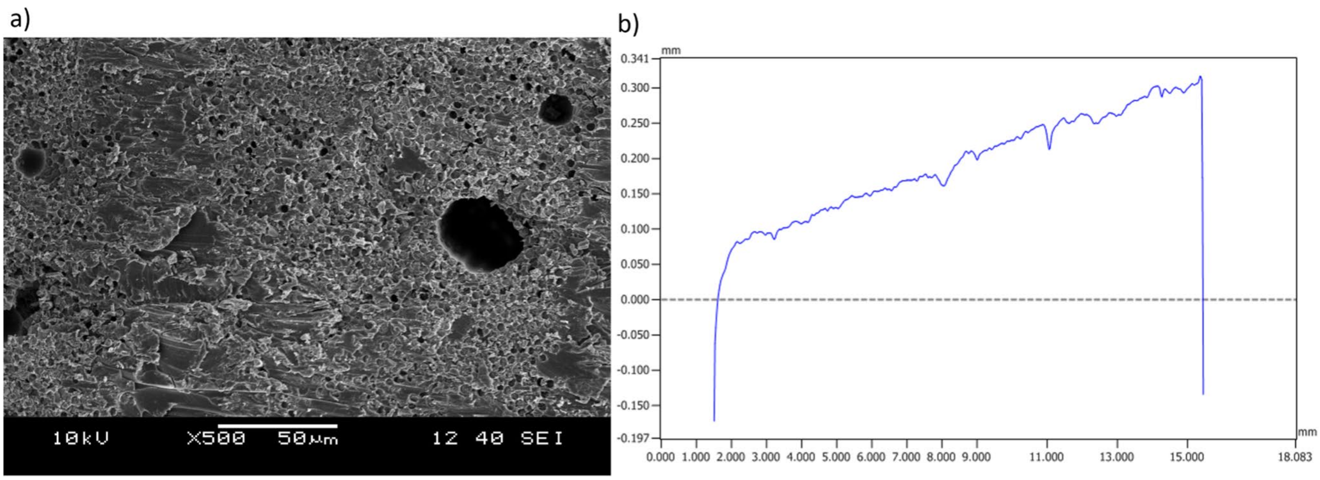

Fig. 4 **a**) SEM micrograph of the raw AWJM surface at 90° fibre orientation, and **b**) 3D surface profile measured perpendicular to the fibre orientation

$F_x(t)$, $F_y(t)$ and $F_z(t)$, corresponding to the feed, tangential and axial force components, respectively. The resultant cutting force is expressed by Eq. (1). For the evaluation of the cutting forces, the 100 (n) largest resultant cutting forces ($\max(Ft)$) were calculated and then averaged to determine the F cutting force, which is used in this study to characterise the processes. The maximum peak cutting force was selected rather than the average force because the onset and propagation of machining-induced damage are governed by the highest instantaneous loads experienced by the material.

$$F(t) = \sqrt{F_x(t)^2 + F_y(t)^2 + F_z(t)^2} \Rightarrow F_t = \sqrt{F_{x,t}{}^2 + F_{y,t}{}^2 + F_{z,t}{}^2} \quad (1)$$

$$F = \frac{1}{n}\sum{}_{i=1}^{n}\max(F_t)_i \quad (2)$$

The surface quality was measured according to the ISO 4288:1996 standard with a Mitutoyo SJ-400 contact profilometer (Fig. 3b), each milling surface 5 times parallel to the feed and then averaged. The surface integrity was photographed by a Dino-Lite Edge AF4515ZT digital microscope (Fig. 3c), and four representative milled surfaces were investigated with a Jeol JSM-6380LA scanning electron microscope (Fig. 3a). A Jeol JFC-1200 FINE COATER was used for the preparation of the SEM investigation.

The experimental results were analysed using analysis of variance (ANOVA) at a significance level of $\alpha = 0.05$. Factors and interactions with p-values below 0.05 were considered statistically significant. Due to the non-linear nature of the cutting mechanisms, fibre orientation was defined as a categorical factor with four discrete levels (0°, 45°, 90°, and 135°) rather than a continuous covariate.

The microscopic condition of the raw AWJM surface prior to machining was characterised. As depicted in the SEM micrograph (Fig. 4a), the preliminary abrasive water jet machining process produced a relatively smooth surface containing only minor cavities, which originated primarily from the laminate manufacturing process rather than from the AWJM operation itself. The macroscopic geometrical accuracy of the AWJ-cut CFRP was evaluated using a Zeiss UC 850 coordinate measuring machine (CMM). The measured flatness deviation of the top surface was 0.177 mm, exhibiting edge rounding caused by intersecting cuts during the initial material separation. Furthermore, a significant perpendicularity error of 0.31 mm was recorded relative to the clamped reference plane. This global inclination is an inherent consequence of the kerf taper effect generated by the preliminary AWJM process. To physically verify this, the 3D surface profile was captured using a Keyence VR 5000 optical microscope. As illustrated in Fig. 4b, the profile clearly demonstrates a continuous slope corresponding to the abrasive water jet divergence, providing definitive proof of the kerf taper effect.

3 Results and discussion

3.1 Cutting force

Representative filtered cutting force diagrams are shown in Fig. 5. The diagrams reveal that the cutting force varies with the chip thickness, and the combined effect of the chip thickness and fibre cutting angle governs mainly the composites' resistance against chip removal. The frequency of the fluctuations in force is attributed to the number of cutting edges of the end milling tool and the spindle speed. The diagrams illustrate a clear trend: as cutting depth and

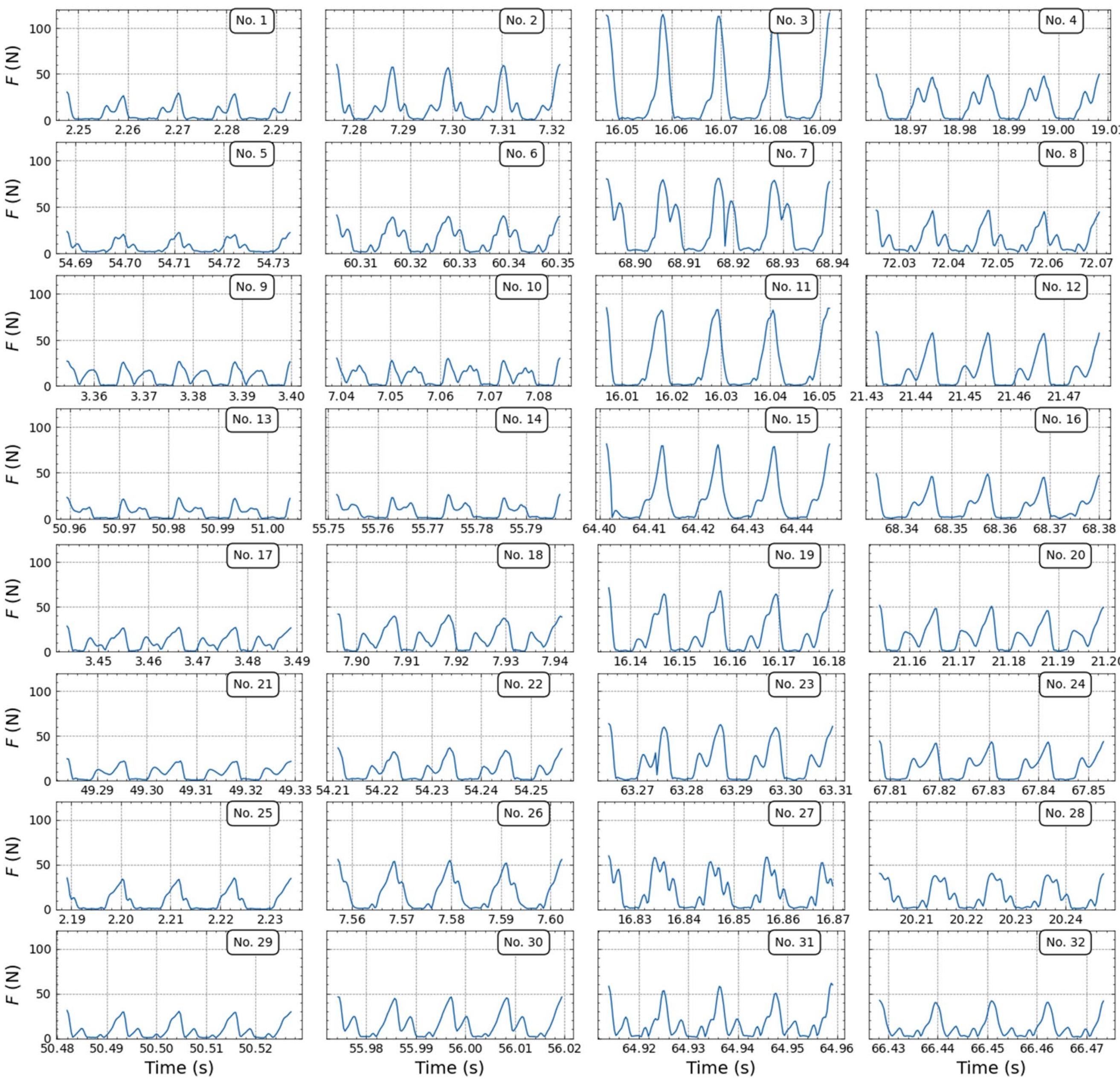

Fig. 5 Representative filtered force diagrams, where the numbers (No. 1 − 32) reflect the experimental run number according to Table A1

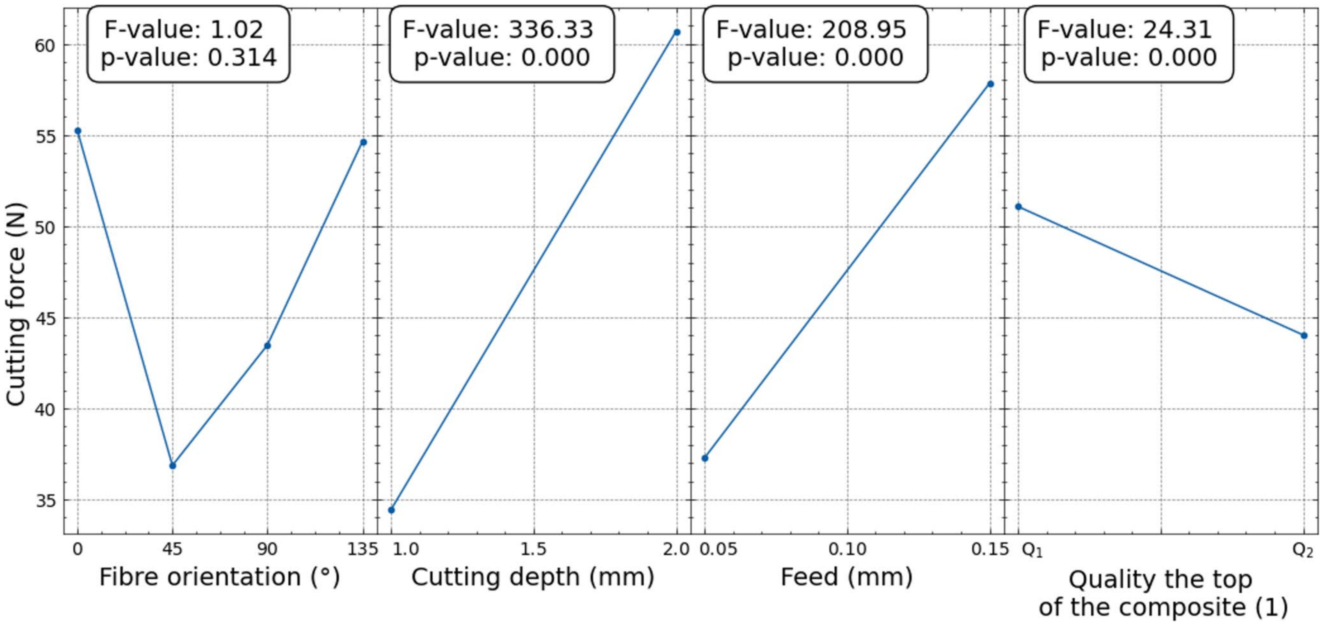

Fig. 6 Main effect plots showing the influence of the factors on the cutting force (*F*)

Table 4 ANOVA table for the cutting force, where bold entries denote p-values lower than $\alpha = 0.05$, indicating that the particular factor has a significant effect

Source	DF	Adj SS	Adj MS	F-value	*p*-value
Model	11	34719.2	3156.3	64.53	0.000
Linear	4	27908.2	6977.0	142.65	0.000
ψ	1	50.1	50.1	1.02	0.314
a_p	1	16449.4	16449.4	336.33	**0.000**
f	1	10219.6	10219.6	208.95	**0.000**
Q	1	1189.1	1189.1	24.31	**0.000**
2-Way Interaction	6	1765.8	294.3	6.02	0.000
$\psi \cdot a_p$	1	76.0	76.0	1.55	0.216
$\psi \cdot f$	1	362.3	362.3	7.41	**0.008**
$\psi \cdot Q$	1	81.5	81.5	1.67	0.200
$a_p \cdot f$	1	1044.2	1044.2	21.35	**0.000**
$a_p \cdot Q$	1	0.0	0.0	0.00	0.978
$f \cdot Q$	1	201.7	201.7	4.12	**0.045**
Error	84	4108.3	48.9		
Total	95	38827.6			

feed increase, the cutting force intensifies, as expected [45]. Additionally, in the case of the pre-machined surface, significantly lower cutting forces were observed compared to the raw surface, suggesting that surface conditions significantly influence force behaviours during machining.

The influence of various factors on the cutting force (*F*) and the corresponding ANOVA results are illustrated in Fig. 6 and Table 4. The main effect plots clearly indicate that cutting depth, quality and feed have a significant impact on cutting force, i.e., as the feed and cutting depth increase, the resultant cutting force also rises, demonstrating that when the machined area per unit time expands, the cutting force proportionally intensifies.

Nevertheless, ANOVA proved that the fibre orientation influence is not significant. It is well known that the fibre orientation is a key parameter affecting chip removal mechanisms of CFRP composites [46]; thus, its influence is expected to be significant. The reason for the observed insignificance is consequently lies in the inconsistent depth of cut when the raw (produced by AWJM) composite is machined, as the significant influence of the quality of the top of the composite on the cutting force suggests the same. Clamping the raw AWJM surface in the CNC vice can introduce specimen misalignment and slanting relative to the spindle. This lack of perpendicularity, combined with macro-geometric waviness, causes unpredictable variations in the actual depth of cut, thereby masking the effect of fibre orientation. We are proving it within this paper and highlighting the importance of the pre-machining of the composite to ensure identical cutting depth along the machining path. To further illustrate the dispersion of the cutting force data and to highlight the increased variability observed on the raw AWJM surface compared to the pre-machined condition, a scatter plot is presented in Fig. 7.

The ANOVA revealed three significant two-way interactions regarding the resultant cutting force. Firstly, the interaction between fibre orientation and feed demonstrates that the sensitivity of cutting forces to feed increments is highly orientation-dependent, with the detrimental effects of critical angles —particularly 135°— being disproportionately amplified at higher feeds. Secondly, between cutting depth and feed indicates a non-linear escalation in force as the

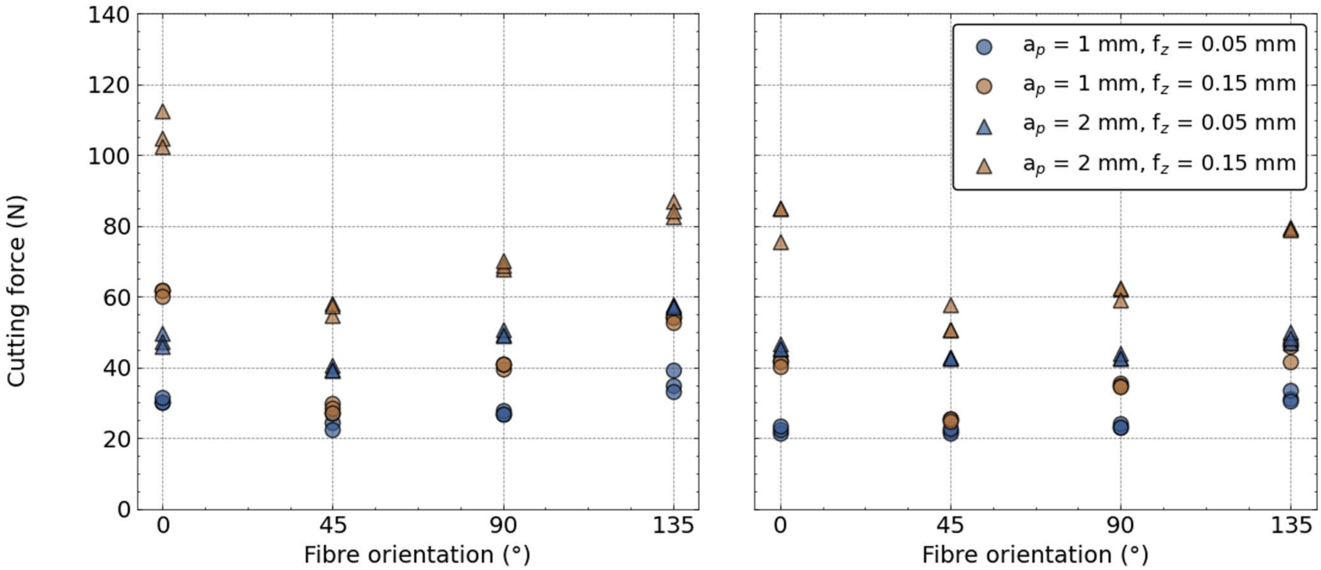

Fig. 7 Scatter plot of cutting force vs. fibre orientation (a_p = 1 mm and a_p = 2 mm) for **a**) AWJM surface (Q_1), and **b**) pre-machined surface (Q_2). The diagrams illustrate the significantly higher data dispersion in the raw condition

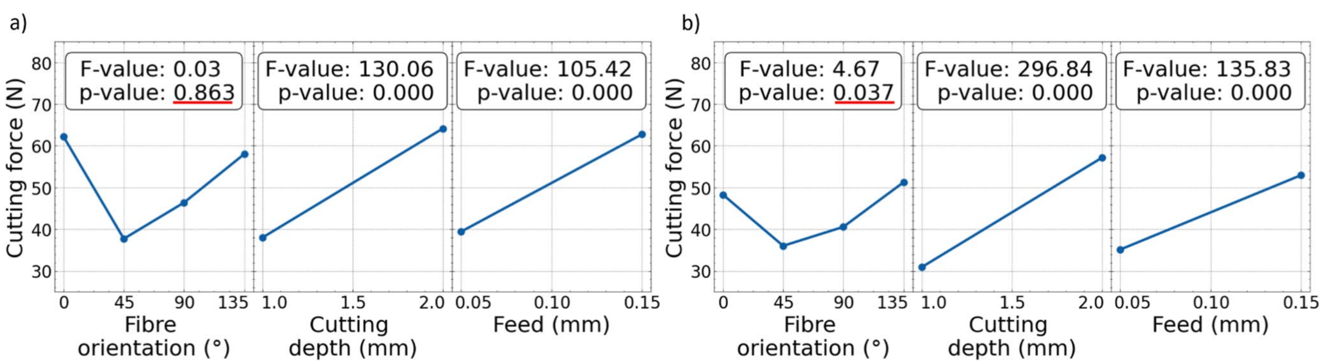

Fig. 8 Main effect plots showing the influence of the factors on the cutting force when the top surface of the composite is **a**) raw and **b**) pre-machined

material removal rate increases, suggesting that the process becomes increasingly sensitive to chip load variations when both parameters are high. Finally, the interaction between feed and top-surface quality provides direct evidence that the initial surface condition fundamentally alters the force response to feed changes; this confirms that pre-machining is indispensable to eliminate the unpredictable variables and inconsistent uncut chip thicknesses (Table 4).

We categorised the dataset based on surface conditions (raw and pre-machined). In this case, a clear distinction in the effect of fibre orientation is observed, as shown in Fig. 8; Table 5. In the case of the raw surface (Fig. 8a), fibre orientation does not exhibit a significant influence on the cutting force (F-value = 0.03, p-value = 0.863). However, for the pre-machined surface (Fig. 8b), fibre orientation plays a more pronounced and significant (F-value = 4.67, p-value = 0.037) role in affecting force behaviour, as expected based on chip removal mechanisms described by many scholars [15, 47]. This proves the importance of pre-machining of CFRP composites before machinability testing in any machining environment such as drilling, edge trimming, flat surface milling, orthogonal cutting. Despite this distinction, cutting depth and feed remain the most influential factors in both cases, consistently exerting a significant impact on the resultant cutting force.

Decomposing the analysis by surface quality reveals distinct force behaviours. In the raw condition (Q_1), inconsistent uncut chip thicknesses drive a significant interaction between fibre orientation and feed. Conversely, mechanical pre-machining (Q_2) eliminates this surface-induced noise, rendering the interaction insignificant and enabling the isolation of true orientation-dependent cutting mechanisms. Notably, the interaction between cutting depth and feed remains highly significant regardless of the initial surface condition. This indicates a persistent, non-linear escalation in cutting force as the material removal rate increases, demonstrating that the process becomes inherently more sensitive to chip load variations when both parameters are elevated.

Table 5 ANOVA tables for the cutting force: (a) raw and (b) pre-machined composites, where bold entries denote p-values lower than α=0.05, indicating that the particular factor has a significant effect

Source	a)	Raw				b)	Pre-machined			
	DF	Adj SS	Adj MS	F-value	*p*-value	DF	Adj SS	Adj MS	F-value	*p*-value
Model	7	19815.6	2830.80	44.9	0.000	7	14189.3	2027.04	72.94	0.000
Linear	3	14848.7	4949.56	78.5	0.000	3	12153.7	4051.24	145.78	0.000
ψ	1	1.9	1.90	0.03	0.863	1	129.7	129.68	4.67	**0.037**
a_p	1	8200.2	8200.20	130.06	**0.000**	1	8249.2	8249.23	296.84	**0.000**
f	1	6646.6	6646.57	105.42	**0.000**	1	3774.8	3774.81	135.83	**0.000**
2-Way interaction	3	1181.3	393.75	6.24	**0.001**	3	520.5	173.5	6.24	**0.001**
$\psi \cdot a_p$	1	18.9	18.94	0.30	0.587	1	63.6	63.60	2.29	0.138
$\psi \cdot f$	1	558.2	558.17	8.85	**0.005**	1	10.8	10.85	0.39	0.536
$a_p \cdot f$	1	604.1	604.14	9.58	**0.004**	1	446.0	446.05	16.05	**0.000**
Error	40	2522.0	63.05			40	1111.6	27.79		
Total	47	22337.6				47	15300.9			

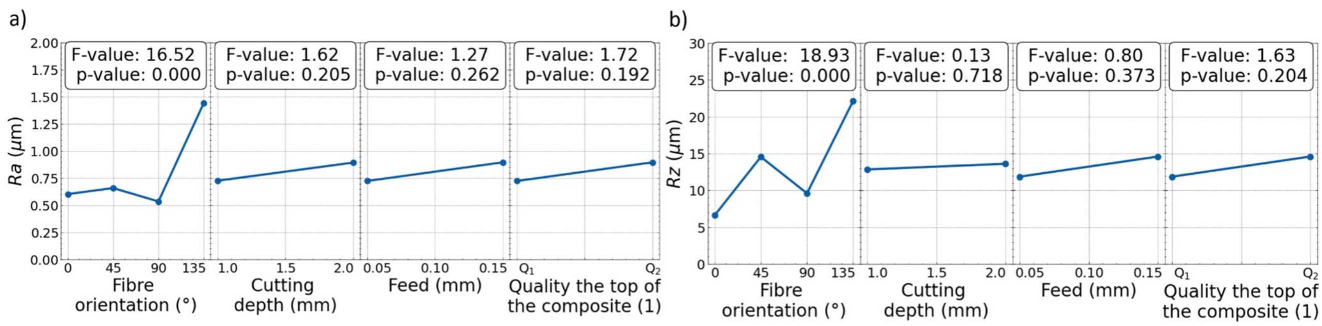

Fig. 9 Main effect plots showing the influence of fibre orientation, cutting depth, feed and top surface quality on the **a**) *Ra* and **b**) *Rz*

3.2 Surface quality

3.2.1 Surface roughness

The average surface roughness (*Ra*) values (0.37–2.08 µm) were consistently relatively low across all tested conditions. Even the highest *Ra* value of 2.08 µm remained within a range considered acceptable for conventional machining processes [48]. In contrast, certain roughness depth (*Rz*) values were found to be relatively high (cc. 31.84 µm), which is attributed to localised surface damage, most notably fibre pull-outs, which are common in the machining of fibre-reinforced composites [32, 49]. ANOVA confirmed that among the investigated parameters, only the fibre orientation had a significant effect on both *Ra* and *Rz* values (Fig. 9). Among the tested orientations, the most favourable surface roughness was achieved at fibre orientations of 0° and 90°, while the poorest surface quality corresponded to a fibre orientation of 135°.

In addition to the surface roughness parameters, a distinct matrix smearing effect was observed on the machined surfaces by the optical and scanning microscope (Fig. 10), which may have had a considerable influence on the profilometric measurements. This smeared layer, formed by the redistribution of the matrix material during machining, contributed to the apparent reduction in surface roughness values —particularly in *Ra* — by partially filling surface irregularities and covering exposed fibres and fibre pull-outs. The smearing was particularly pronounced due to the high thermal loads generated during the machining process. During the face milling process, the continuous engagement between the cutting tool and the workpiece surface resulted in localised temperature elevations, which in turn softened the matrix material. As a result, the softened matrix was deformed and smeared over the surface [50, 51].

Importantly, the extent of matrix smearing was found to be strongly influenced by the fibre orientation. Different fibre orientations affect how the cutting tool interacts with the composite structure [24, 52], which in turn governs the way the softened matrix material is redistributed on the surface. Orientations that resulted in more favourable cutting conditions allowed the matrix to be smeared more uniformly over the surface, contributing to a smoother measured profile. The presence of the smeared matrix layer, while contributing to a lower apparent roughness, may also have masked subsurface features such as fibre pull-outs or microcracks, as pointed out previously by Ashworth et al. [53]. As the contact profilometer records the topography of this smeared surface layer, the measured values may not fully reflect the true underlying surface condition (Table 6).

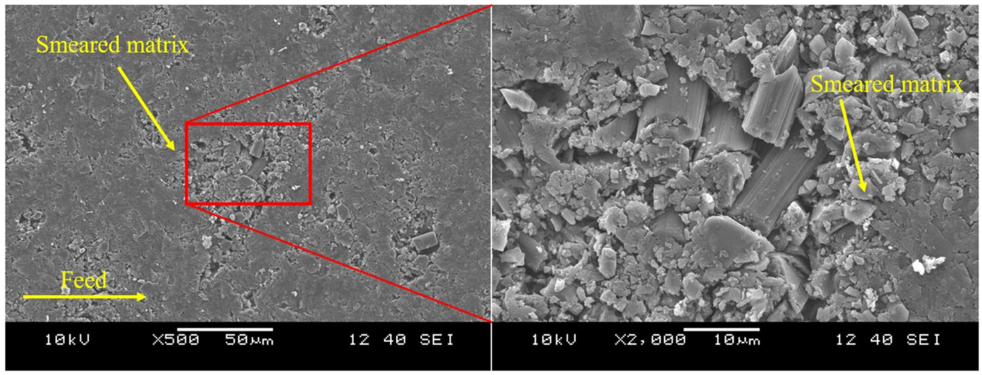

Fig. 10 Representative SEM image of significant matrix smearing

Table 6 ANOVA tables for (a) *Ra* and (b) *Rz*, where bold entries denote p-values lower than α = 0.05, indicating that the particular factor has a significant effect

	a)	*Ra*				b)	*Rz*			
Source	DF	Adj SS	Adj MS	F-value	*p*-value	DF	Adj SS	Adj MS	F-value	*p*-value
Model	11	24.5	2.22	3.2	0.001	11	4690.5	426.41	2.32	0.012
Linear	4	14.7	3.67	5.28	0.001	4	3945.5	986.36	5.37	0.000
ψ	1	11.5	11.48	16.52	**0.000**	1	3475.7	3475.70	18.93	**0.000**
a_p	1	1.1	1.12	1.62	0.205	1	23.9	23.95	0.13	0.718
f	1	0.9	0.88	1.27	0.262	1	146.9	146.88	0.8	0.373
Q	1	1.192	1.19	1.72	0.192	1	298.9	298.94	1.63	0.204
2-Way Interaction	6	2.529	0.42	0.61	0.725	6	531.9	88.64	0.48	0.820
$\psi \cdot a_p$	1	0.763	0.76	1.10	0.296	1	0.0	0.02	0.00	0.992
$\psi \cdot f$	1	0.305	0.30	0.44	0.509	1	6.5	6.46	0.04	0.851
$\psi \cdot Q$	1	0.010	0.01	0.01	0.903	1	17.5	17.49	0.10	0.758
$a_p \cdot f$	1	0.243	0.24	0.35	0.556	1	18.4	18.43	0.10	0.752
$a_p \cdot Q$	1	1.051	1.05	1.51	0.221	1	479.2	479.21	2.61	0.108
$f \cdot Q$	1	0.157	0.16	0.23	0.635	1	10.3	10.25	0.06	0.814
Error	148	102.864	0.695			148	27171.7	183.59		
Total	159	127.332				159	31862.2			

When categorising the dataset based on surface condition (raw vs. pre-machined), the ANOVA results (Table 7) indicated that the depth of cut had a more noticeable effect on surface roughness when the top surface of the composite was machined (Fig. 11). This is likely due to the more consistent material removal conditions provided by the pre-machined surface, which allowed the cutting depth to remain more permanent throughout the process. Nevertheless, fibre orientation remained the most statistically significant factor affecting surface roughness in all cases.

In contrast to the force results, the analysis of surface roughness (*Ra* and *Rz*) revealed no significant two-way interactions between any of the investigated parameters. While the cutting force is subject to complex parameter, surface topography is primarily governed by fibre orientation. These findings confirm that at the investigated levels, the fundamental fibre-failure mechanisms —such as fibre pull-out, fragmentation, and matrix smearing— associated with specific orientation angles dominate the resulting surface geometry regardless of adjustments to the feed, cutting depth, or initial surface preparation. Similarly, the analysis categorised by surface quality revealed no significant interactions regarding surface roughness. For a more comprehensive evaluation of the surface topography, the supplementary roughness parameters (root mean square roughness (*Rq*), total height of the profile (*Rt*), maximum profile peak height (*Rp*), maximum profile valley depth (*Rv*), and mean spacing of profile elements (*RSm*)) are presented in Table A2 in the Appendix.

3.2.2 Surface integrity

The influence of fibre orientation (0°, 45°, 90°, and 135°) on the resulting surface morphology of the machined composite was systematically investigated using optical microscopy and scanning electron microscopy (SEM). The representative examined specimens (No. 5, 13, 21, and 29 according to Table A1) exhibited surfaces that were generally quasi-homogeneous in appearance, predominantly characterised by smeared matrix material. This matrix smearing was clearly visible in Fig. 12 and may have covered many of the finer microstructural details, such as micro-cracks and

Table 7 ANOVA tables for (a,b) *Ra* and (c,d) *Rz* categorised by the quality of the top of the composite, where bold entries denote p-values lower than α = 0.05, indicating that the particular factor has a significant effect

Ra	a)	Raw				b)	Pre-machined			
Source	DF	Adj SS	Adj MS	F-value	p-value	DF	Adj SS	Adj MS	F-value	p-value
Model	7	12.2	1.74	3.8	0.001	7	12.9	1.85	1.96	0.073
Linear	3	6.3	2.10	4.57	0.005	3	8.4	2.80	2.97	0.037
ψ	1	5.4	5.40	11.77	**0.001**	1	6.1	6.09	6.45	**0.013**
a_p	1	0.0	0.00	0	0.971	1	2.2	2.17	2.3	0.133
f	1	0.9	0.89	1.94	0.168	1	0.1	0.15	0.16	0.694
2-Way interaction	3	1.9	0.6	1.38	0.255	3	1.3	0.4	0.44	0.723
$\psi \cdot a_p$	1	0.05	0.05	0.11	0.743	1	1.03	1.03	1.09	0.301
$\psi \cdot f$	1	1.5	1.5	3.35	0.071	1	0.2	0.2	0.22	0.638
$a_p \cdot f$	1	0.3	0.3	0.69	0.410	1	0.02	0.02	0.02	0.890
Error	72	33.0431	0.45893			72	67.9559	0.94383		
Total	79	45.2426				79	80.8972			
Rz	c)	Raw				d)	Pre-machined			
Source	DF	Adj SS	Adj MS	F-value	p-value	DF	Adj SS	Adj MS	F-value	p-value
Model	7	2614.6	373.51	3.11	0.006	7	2038.0	291.14	1.15	0.344
Linear	3	2255.0	751.67	6.27	0.001	3	1898.5	632.83	2.49	0.067
ψ	1	1993.2	1993.18	16.62	**0.000**	1	1500.0	1500.01	5.91	**0.018**
a_p	1	144.5	144.45	1.2	0.276	1	358.7	358.70	1.41	0.238
f	1	117.4	117.37	0.98	0.326	1	39.8	39.76	0.16	0.693
2-Way interaction	3	126.7	42.23	0.35	0.788	3	110.5	36.82	0.15	0.933
$\psi \cdot a_p$	1	79.8	79.83	0.67	0.417	1	83.2	83.17	0.33	0.569
$\psi \cdot f$	1	43.6	43.63	0.36	0.548	1	9.1	9.06	0.04	0.851
$a_p \cdot f$	1	3.2	3.24	0.03	0.870	1	18.2	18.24	0.07	0.789
Error	72	8633.8	119.91			72	18276.9	253.85		
Total	79	11248.4				79	20314.9			

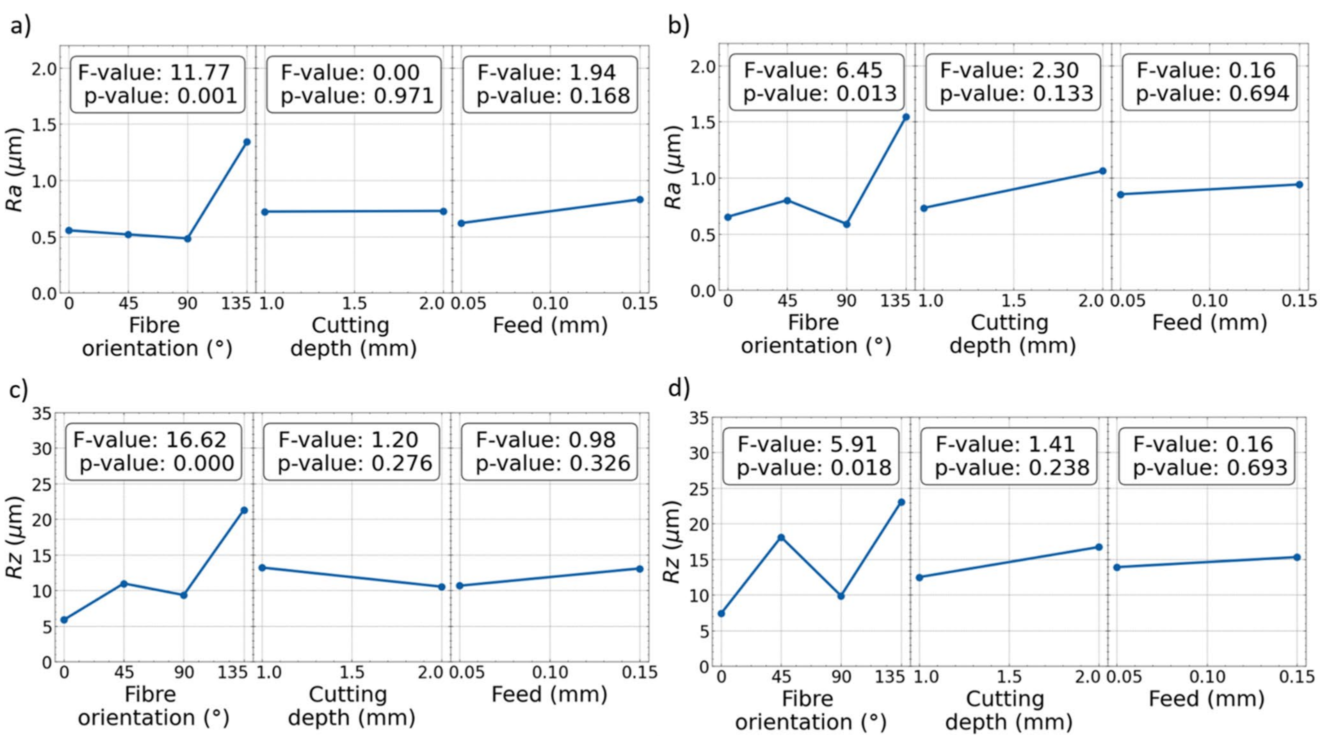

Fig. 11 Main effect plots showing the influence of the factors on the **a)b**) *Ra* and the **c)d**) *Rz* when the top surface of the composite is a)c) raw and b)d) pre-machined

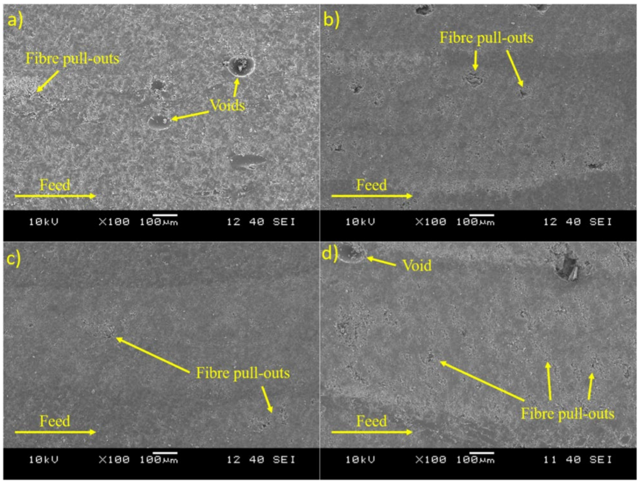

Fig. 12 Representative surface morphologies at different fibre orientations: **a**) 0°, **b**) 45°, **c**) 90°, and **d**) 135°

small cavities originating from fibre pull-out. The limited occurrence of fibre debris and pull-outs across most of the surface further suggests that matrix smearing plays a critical role in concealing or mitigating the visible impact of certain damage mechanisms.

For specimens with fibres oriented at 0° (i.e., fibres aligned parallel to the feed direction), the machined surfaces were relatively smooth, with only occasional fibre pull-outs. When pull-outs occurred, fibres tended to be extracted along substantial lengths. In these instances, the matrix material was unable to fully conceal the resultant voids, leading to visible surface discontinuities, as shown in Fig. 13. Such defects not only compromise surface integrity but could also act as initiation sites for further damage during service loading.

At a fibre orientation of 45°, the overall surface quality was comparable to that observed at 0°. However, fractured fibres were more frequently detected (see Fig. 13b), likely due to partial cutting or ineffective shearing of fibres inclined to the cutting direction. The diagonal fibre alignment appeared to restrict the matrix's ability to flow and smear effectively, thereby reducing its capacity to mask subsurface damage. This suggests that, beneath the visibly smeared surface layer, hidden damage — such as fibre-matrix debonding or micro-cracking — may exist due to incomplete fibre support and ineffective load transfer during cutting. Similar phenomena have been reported in the literature [54, 55], where off-axis fibre orientations are associated with elevated cutting forces and increased likelihood of subsurface damage.

Machined surfaces produced at a fibre orientation of 90° (fibres perpendicular to the feed direction) exhibited the most homogeneous and defect-minimal morphology among the tested configurations. Fibre pull-out was

Fig. 13 Surface morphology with magnified views at different fibre orientations: (**a**) 0°, (**b**) 45°, **c**)**d**) 90 °, and **e**)**f**) 135°

markedly reduced compared to the 0° and 45° cases. In several instances, cut fibre debris was observed to be pushed into the matrix; however, the adhesion of these fibres is not as good as the others within the composite, thus resulting in less effective strength. Nevertheless, complete matrix coverage was not always achieved, and isolated fibre ends remained exposed (Fig. 13c and d). The superior surface quality at 90° fibre orientation may be attributed to more efficient cutting of individual fibres and reduced tendency for fibre pull-out due to the transverse orientation relative to the cutting path.

The most severe surface damage was recorded at the fibre orientation of 135°. In this configuration, fibres were highly misaligned relative to the cutting direction, resulting in substantial fibre bundle pull-out, severe fibre fragmentation, and extensive breakage (Fig. 13e and f). The matrix's ability to smear and cover damaged regions was significantly impaired; both the fragmented fibres and displaced matrix material were redistributed across the machined surface, giving rise to a markedly irregular and disrupted morphology. Such extensive damage is indicative of complex failure modes involving combined fibre fracture, interfacial debonding, and matrix tearing, all of which contribute to degraded surface integrity and potentially compromised mechanical performance.

These observations collectively underscore that fibre orientation exerts a significant influence on machined surface quality. As the fibre orientation is closer to 90°, the surface quality is expected to be good, while the surface damage mechanisms become progressively more complex, involving a combination of fibre pull-out, breakage, and diminished matrix smearing at larger fibre orientations. This highlights the importance of tailoring machining strategies to fibre architecture in order to minimise surface defects and preserve composite integrity. These observed micromechanical failure modes—specifically severe fibre pull-out, matrix smearing, and interfacial debonding—are in strong agreement with the characteristic machining-induced morphological defects comprehensively documented in recent SEM evaluations of FRP composites [5, 51].

4 Conclusions

In the present study, the effects of process parameters of face milling and top surface quality of composites on the surface quality and integrity of carbon fibre reinforced polymer (CFRP) composites were examined, along with the investigation of cutting force. According to the present study, the following conclusions can be drawn:

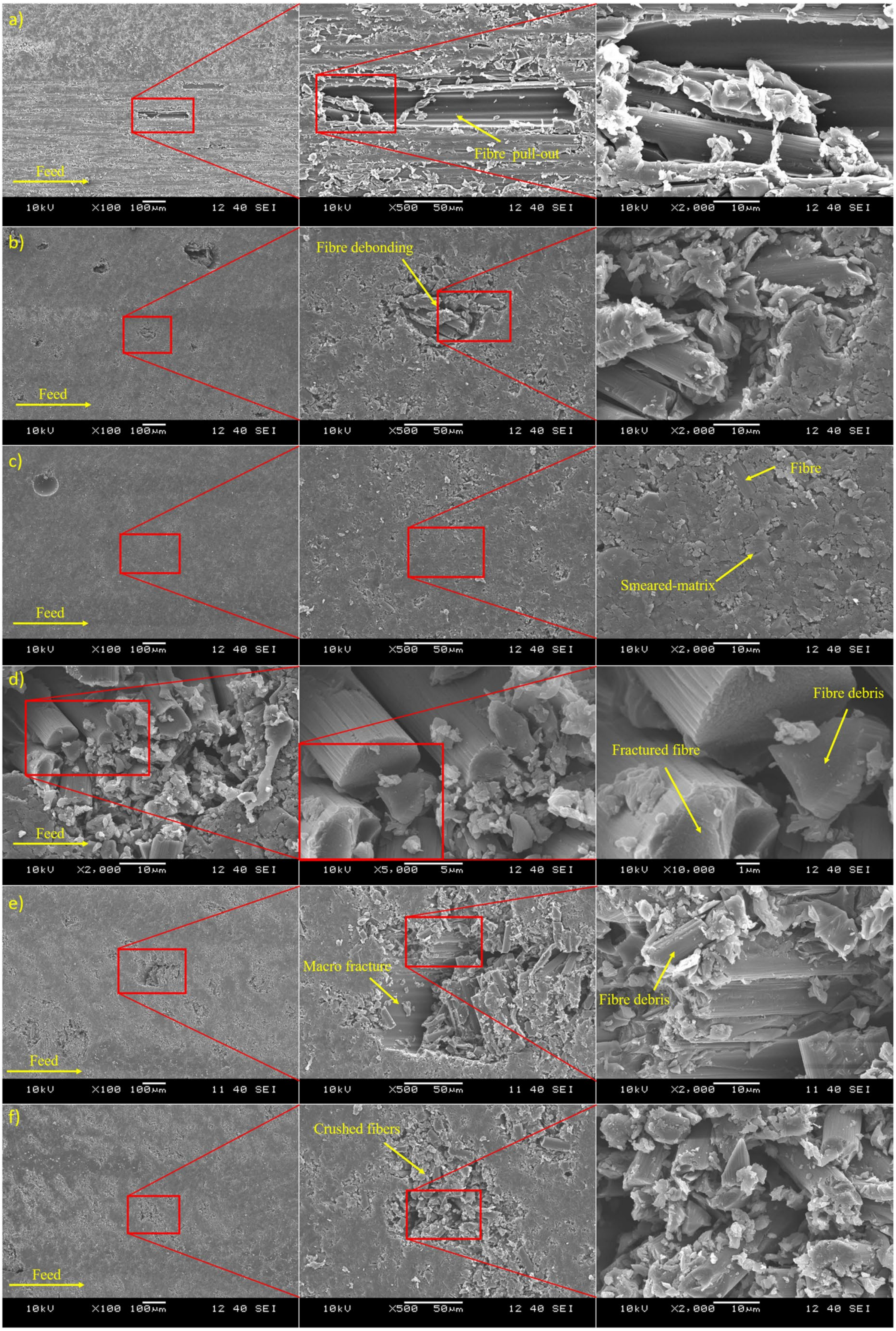
a)
Feed
Fibre pull-out
10kV X100 100μm 12 40 SEI
10kV X500 50μm 12 40 SEI
10kV X2,000 10μm 12 40 SEI
b)
Feed
Fibre debonding
c)
Feed
Fibre
Smeared-matrix
d)
Feed
Fibre debris
Fractured fibre
10kV X2,000 10μm 12 40 SEI
10kV X5,000 5μm 12 40 SEI
10kV X10,000 1μm 12 40 SEI
e)
Feed
Macro fracture
Fibre debris
10kV X100 100μm 11 40 SEI
10kV X500 50μm 11 40 SEI
10kV X2,000 10μm 11 40 SEI
f)
Feed
Crushed fibers

- ANOVA results show that the influence of the feed and the depth of cut is significant, while the influence of the fibre direction is not significant on the cutting force when the top surface of the CFRP specimens were prepared by AWJC technology (Q_1). However, if the top surface of the CFRP specimens were prepared by machining technology (Q_2), the influence of the fibre orientation becomes statistically significant, as expected. It suggests that an inconsistent preparation of the top surface of the CFRP specimen results in inconsistent uncut chip thickness, thus the influence of fibre orientation is not comparable to the expectations (i.e., the influence of the fibre direction is significant).
- Experimental results proved that mechanical machining of the top of CFRP specimens is required before conducting machining experiments to maintain the uniform allowance (chip thickness) that is essential in order to gain relevant information on the proper influence of fibre direction on the cutting force. It was also shown that milling with optimal conditions ensures good surface quality; thus, the milling-induced geometrical defects (e.g., delamination, matrix smearing, cracks, etc.) will not influence the machining results significantly.
- Surface roughness investigations showed that (i) optimal surface quality is achievable at 0° and 90° of fibre orientation, and (ii) it is recommended to avoid the cutting condition when the fibre orientation angle is 135° in order to minimise the possibility of macrofracture and fibre pull-out on the machined surface, resulting in poor surface quality. In addition, a significant matrix smearing was observed in the SEM images at every fibre orientation angle that may cover potential micro-damages such as microcracks. Considering that good surface quality does not necessarily guarantee the appropriate mechanical properties of the material, as micro-geometric defects may occur beneath the smeared matrix. Therefore, the authors will investigate the mechanical properties and the subsurface quality of the milled UD-CFRP composites in the future.
- Uncontrolled top-surface variability can obscure physically meaningful machining phenomena. Although fibre orientation is known to govern CFRP chip-removal mechanisms, its effect on cutting force became statistically significant only after establishing a uniform allowance by pre-machining. Therefore, specimen preparation should be regarded as a critical experimental variable in CFRP machinability studies.

Appendix 1

No. (1)	ψ (°)	a_p (mm)	f (mm)	Q (1)	F ± s* (*N*)	Ra ± s* (µm)	Rz ± s* (µm)
1	0	1	0.05	1	24.32 ± 1.23	0.54 ± 0.11	5.54 ± 1.64
2	0	1	0.15	1	41.41 ± 2.56	0.52 ± 0.29	6.74 ± 3.98
3	0	2	0.15	1	87.81 ± 4.57	0.57 ± 0.27	5.98 ± 3.42
4	0	2	0.05	1	44.97 ± 1.15	0.59 ± 0.27	5.20 ± 2.57
5	0	1	0.05	2	23.16 ± 0.78	0.49 ± 0.23	5.04 ± 1.43
6	0	1	0.15	2	41.13 ± 1.81	0.58 ± 0.16	6.34 ± 3.44
7	0	2	0.15	2	82.89 ± 5.21	0.98 ± 1.10	12.00 ± 15.21
8	0	2	0.05	2	45.96 ± 1.13	0.56 ± 0.26	6.12 ± 4.16
9	45	1	0.05	1	25.10 ± 0.91	0.58 ± 0.53	10.02 ± 12.85
10	45	1	0.15	1	31.97 ± 2.59	0.59 ± 0.13	13.52 ± 9.57
11	135	2	0.15	1	88.30 ± 3.19	2.04 ± 4.11	21.84 ± 24.03
12	135	2	0.05	1	56.96 ± 2.03	0.83 ± 0.75	14.50 ± 21.08
13	45	1	0.05	2	22.01 ± 1.15	0.67 ± 0.68	15.68 ± 21.06
14	45	1	0.15	2	25.22 ± 1.47	0.74 ± 0.99	16.38 ± 24.77
15	135	2	0.15	2	78.92 ± 3.34	2.08 ± 3.37	31.84 ± 57.20
16	135	2	0.05	2	48.69 ± 1.70	2.03 ± 5.36	25.84 ± 65.09
17	90	1	0.05	1	25.62 ± 0.82	0.54 ± 0.44	11.50 ± 18.49
18	90	1	0.15	1	39.80 ± 2.11	0.51 ± 0.27	9.58 ± 13.69
19	90	2	0.15	1	57.12 ± 2.87	0.51 ± 0.27	8.92 ± 10.17
20	90	2	0.05	1	41.79 ± 1.13	0.37 ± 0.24	7.40 ± 13.80
21	90	1	0.05	2	23.41 ± 1.12	0.48 ± 0.12	8.72 ± 1.97
22	90	1	0.15	2	34.65 ± 1.62	0.81 ± 1.06	13.26 ± 20.66

No. (1)	ψ (°)	a_p (mm)	f (mm)	Q (1)	F ± s* (*N*)	Ra ± s* (µm)	Rz ± s* (µm)
23	90	2	0.15	2	60.99 ± 3.34	0.54 ± 0.30	8.60 ± 7.72
24	90	2	0.05	2	43.19 ± 1.29	0.52 ± 0.51	8.90 ± 12.49
25	135	1	0.05	1	37.12 ± 0.80	1.06 ± 2.24	21.76 ± 56.61
26	135	1	0.15	1	63.39 ± 2.20	1.44 ± 1.05	27.06 ± 27.23
27	45	2	0.15	1	53.19 ± 6.26	0.46 ± 0.24	11.02 ± 16.80
28	45	2	0.05	1	36.71 ± 1.32	0.45 ± 0.18	9.36 ± 11.06
29	135	1	0.05	2	32.02 ± 2.17	1.17 ± 1.68	19.60 ± 30.61
30	135	1	0.15	2	45.39 ± 2.59	0.91 ± 0.53	14.88 ± 12.32
31	45	2	0.15	2	54.26 ± 4.83	0.88 ± 0.54	19.18 ± 19.77
32	45	2	0.05	2	42.54 ± 1.17	0.90 ± 1.54	21.30 ± 43.01

Appendix 2

No. (1)	ψ (°)	a_p (mm)	f (mm)	Q (1)	Rq ± s* (*N*)	Rt ± s* (µm)	Rp ± s* (µm)	Rv ± s* (µm)	RSm ± s* (µm)
1	0	1	0.05	1	0.74 ± 0.11	5.54 ± 0.92	3.24 ± 1.21	2.26 ± 0.96	210.52 ± 76.23
2	0	1	0.15	1	0.75 ± 0.24	6.74 ± 2.22	3.68 ± 1.76	3.06 ± 2.18	333.14 ± 223.11
3	0	2	0.15	1	0.77 ± 0.22	5.98 ± 1.91	3.64 ± 1.32	2.32 ± 1.11	203.5 ± 56.43
4	0	2	0.05	1	0.76 ± 0.19	5.2 ± 1.44	2.76 ± 0.87	2.42 ± 0.85	200.28 ± 38.99
5	0	1	0.05	2	0.68 ± 0.16	5.04 ± 0.8	2.76 ± 0.39	2.28 ± 0.65	212.76 ± 84.77
6	0	1	0.15	2	0.77 ± 0.1	6.34 ± 1.92	3.68 ± 1.34	2.68 ± 0.81	234.6 ± 104.07
7	0	2	0.15	2	1.52 ± 1.08	12 ± 8.51	5.76 ± 2.7	6.24 ± 5.89	352.72 ± 184.57
8	0	2	0.05	2	0.78 ± 0.25	6.12 ± 2.32	2.86 ± 1.01	3.24 ± 1.59	268.08 ± 147.02
9	45	1	0.05	1	1.02 ± 0.73	10.02 ± 7.18	5.1 ± 2.92	4.96 ± 5.43	368.84 ± 440.99
10	45	1	0.15	1	1.05 ± 0.31	13.52 ± 5.35	4.7 ± 2	8.82 ± 6.78	344.48 ± 60.71
11	135	2	0.15	1	2.84 ± 2.78	21.84 ± 13.43	9.78 ± 5.76	12.02 ± 7.75	370.6 ± 412.33
12	135	2	0.05	1	1.44 ± 1.02	14.5 ± 11.78	5.76 ± 2.68	8.76 ± 10.42	614.66 ± 936.24
13	45	1	0.05	2	1.47 ± 1.1	15.68 ± 11.77	8.22 ± 6.94	7.44 ± 10.66	546.48 ± 526.35
14	45	1	0.15	2	1.39 ± 1.24	16.38 ± 13.85	6.28 ± 2.83	10.1 ± 11.84	542.28 ± 312.76
15	135	2	0.15	2	3.69 ± 3.82	31.84 ± 31.97	12.22 ± 11.28	19.62 ± 20.84	382.66 ± 330.66
16	135	2	0.05	2	3.15 ± 4.89	25.84 ± 36.39	10.36 ± 13.52	15.52 ± 22.96	221.2 ± 63.53
17	90	1	0.05	1	1.02 ± 0.76	11.5 ± 10.34	6.92 ± 4.96	4.58 ± 5.5	387.73 ± 202.4
18	90	1	0.15	1	0.93 ± 0.55	9.58 ± 7.65	5.56 ± 5.73	4 ± 4.93	214.66 ± 218.96
19	90	2	0.15	1	0.85 ± 0.36	8.92 ± 5.69	3.62 ± 0.97	5.28 ± 5.27	862.96 ± 1014.06
20	90	2	0.05	1	0.66 ± 0.48	7.4 ± 7.72	3.54 ± 1.61	3.86 ± 6.28	134.6 ± 20.75
21	90	1	0.05	2	0.77 ± 0.08	8.72 ± 1.1	4.68 ± 1.1	4.02 ± 1.61	389.92 ± 90.55
22	90	1	0.15	2	1.49 ± 1.38	13.26 ± 11.55	7.74 ± 6.65	5.52 ± 5	286.75 ± 337.38
23	90	2	0.15	2	0.81 ± 0.28	8.6 ± 4.32	4.4 ± 1.08	4.18 ± 3.85	296.68 ± 247.68
24	90	2	0.05	2	0.86 ± 0.65	8.9 ± 6.99	3.42 ± 0.91	5.46 ± 6.47	277.06 ± 160.57
25	135	1	0.05	1	2.2 ± 3.25	21.76 ± 31.64	8.74 ± 11.84	13.04 ± 19.93	180.08 ± 64.95
26	135	1	0.15	1	2.67 ± 1.37	27.06 ± 15.22	7.56 ± 3.21	19.48 ± 12.31	351.23 ± 130.46
27	45	2	0.15	1	0.86 ± 0.55	11.02 ± 9.39	6.7 ± 8.5	4.32 ± 2.63	285.23 ± 219.89
28	45	2	0.05	1	0.84 ± 0.39	9.36 ± 6.18	5.76 ± 4.13	3.58 ± 2.22	289.73 ± 168.37
29	135	1	0.05	2	2.37 ± 2.29	19.6 ± 17.11	7.54 ± 4.29	12.02 ± 12.94	422.3 ± 273.56
30	135	1	0.15	2	1.51 ± 0.63	14.88 ± 6.89	6 ± 1.74	8.9 ± 5.66	340.92 ± 214.71
31	45	2	0.15	2	1.7 ± 0.9	19.18 ± 11.05	8.1 ± 5.05	11.06 ± 7.87	461.56 ± 254.26
32	45	2	0.05	2	2.01 ± 2.43	21.3 ± 24.04	6.92 ± 5.31	14.38 ± 18.76	372.97 ± 66.38

Acknowledgements This research was partly supported by the János Bolyai Research Scholarship of the Hungarian Academy of Sciences No. BO/00508/22/6 and has been implemented with the support provided by the Ministry of Culture and Innovation of Hungary from the National Research, Development and Innovation Fund, financed under the EKÖP-24-4-II-BME-157 funding scheme. This research was implemented thanks to the support of the 2024 − 1.2.5-TÉT-2024-00032, which encourages scientific and technological cooperation between China and Hungary. The authors acknowledge the support of Dánel István Poór, Dóra Károly, Levente Zsóka, József Hlinka, Dávid Kálmán, Balázs Gábor Pinke, Tamás Sándor Tima, and Mátyás Belső in the experimental work.

Authors' contributions Levente Bukor: Conceptualization, Investigation, Methodology, Formal analysis, Visualization, Writing - Original Draft; Norbert Geier: Conceptualization, Methodology, Investigation, Writing - Original Draft; Rao Fu: Writing – Review and Editing.

Funding Open access funding provided by Budapest University of Technology and Economics. Not applicable.

Data availability The data that support the findings of this study are available from the corresponding author, upon reasonable request.

Code availability Not applicable.

Declarations

Ethics approval Not applicable.

Consent to participate Not applicable.

Consent for publication Not applicable.

Declaration of generative AI and AI-assisted technologies in the writing process During the preparation of this work, the authors used ChatGPT and Copilot in order to improve the English text. After using this tool, the authors reviewed and edited the content as needed and take full responsibility for the content of the publication.

Conflicts of interest/Competing interests Not applicable.

References

1. Kong K, Dyer K, Payne C et al (2023) Progress and Trends in Damage Detection Methods, Maintenance, and Data-driven Monitoring of Wind Turbine Blades – A Review. Renew Energy Focus 44:390–412. https://doi.org/10.1016/j.ref.2022.08.005
2. Shu L, Li S, Fang Z et al (2021) Study on dedicated drill bit design for carbon fiber reinforced polymer drilling with improved cutting mechanism. Compos Part Appl Sci Manuf 142:106259. https://doi.org/10.1016/j.compositesa.2020.106259
3. Pohasii S, Milevskyi S, Brynza N, Vilkhivska O (2025) Prospects for the Development of UAVs Using CFRP and 3D Printing. In: Durakbasa NM, Cetinkaya K, Demircioglu P, Bogrekci I (eds) Digitalization in Additive Manufacturing. Springer Nature Switzerland, Cham, pp 323–333
4. Bharath KN, Joshi AG, Taj A et al (2025) Chap. 9 - Evolution and recent advancements of composite materials in sports applications. In: Puttegowda M, Gowda T.G. Y, J.s. B, (eds) Applications of Composite Materials in Engineering. Elsevier Science Ltd, pp 219–228
5. Vedernikov A, Gemi L, Madenci E et al (2022) Effects of high pulling speeds on mechanical properties and morphology of pultruded GFRP composite flat laminates. Compos Struct 301:116216. https://doi.org/10.1016/j.compstruct.2022.116216
6. Özkılıç YO, Madenci E, Safonov A et al (2025) Comprehensive evaluation of tensile properties, damage mechanisms, and predictive modeling of pultruded GFRP after elevated temperatures. Compos Part B Eng 304:112657. https://doi.org/10.1016/j.compositesb.2025.112657
7. Geier N (2025) Fibre-orientation-driven defect probability mapping for machining-induced delamination and burr minimisation in carbon fibre-reinforced polymer (CFRP) composites. Compos Part C Open Access 18:100636. https://doi.org/10.1016/j.jcomc.2025.100636
8. Davim JP (2013) Machining Composites Materials. Wiley
9. Xu J, Li C, Mi S et al (2018) Study of drilling-induced defects for CFRP composites using new criteria. Compos Struct 201:1076–1087. https://doi.org/10.1016/j.compstruct.2018.06.051
10. Jia Z, Fu R, Niu B et al (2016) Novel drill structure for damage reduction in drilling CFRP composites. Int J Mach Tools Manuf 110:55–65. https://doi.org/10.1016/j.ijmachtools.2016.08.006
11. Doğan MA, Yazman Ş, Gemi L et al (2022) A review on drilling of FML stacks with conventional and unconventional processing methods under different conditions. Compos Struct 297:115913. https://doi.org/10.1016/j.compstruct.2022.115913
12. Gemi L, Morkavuk S, Köklü U, Gemi DS (2019) An experimental study on the effects of various drill types on drilling performance of GFRP composite pipes and damage formation. Compos Part B Eng 172:186–194. https://doi.org/10.1016/j.compositesb.2019.05.023
13. An Q, Cai C, Cai X, Chen M (2019) Experimental investigation on the cutting mechanism and surface generation in orthogonal cutting of UD-CFRP laminates. Compos Struct 230:111441. https://doi.org/10.1016/j.compstruct.2019.111441
14. Wang F, Yin J, Ma J, Niu B (2018) Heat partition in dry orthogonal cutting of unidirectional CFRP composite laminates. Compos Struct 197:28–38. https://doi.org/10.1016/j.compstruct.2018.05.040
15. Li H, Qin X, He G et al (2016) Investigation of chip formation and fracture toughness in orthogonal cutting of UD-CFRP. Int J Adv Manuf Technol 82:1079–1088. https://doi.org/10.1007/s00170-015-7471-x
16. An Q, Zhang J, Xiao G et al (2025) Fiber Orientation Effects in CFRP Milling: Multiscale Characterization of Cutting Dynamics, Surface Integrity, and Damage Mechanisms. J Compos Sci 9:342. https://doi.org/10.3390/jcs9070342
17. Chen J, An Q, Chen M et al (2025) Digital twin dynamic force-thermal physics sub-cell for CFRP drilling process. Compos Part B Eng 292:112057. https://doi.org/10.1016/j.compositesb.2024.112057
18. Gemi L, Köklü U, Yazman Ş, Morkavuk S (2020) The effects of stacking sequence on drilling machinability of filament wound hybrid composite pipes: Part-1 mechanical characterization and

drilling tests. Compos Part B Eng 186:107787. https://doi.org/10.1016/j.compositesb.2020.107787
19. Morkavuk S, Aslantaş K, Gemi L et al (2024) The influence of drilling-induced damages and hole quality on hoop tensile and fatigue behavior of CFRP tubes. Compos Part Appl Sci Manuf 179:108005. https://doi.org/10.1016/j.compositesa.2024.108005
20. Wang XM, Zhang LC (2003) An experimental investigation into the orthogonal cutting of unidirectional fibre reinforced plastics. Int J Mach Tools Manuf 43:1015–1022. https://doi.org/10.1016/S0890-6955(03)00090-7
21. Wang C, Liu G, An Q, Chen M (2017) Occurrence and formation mechanism of surface cavity defects during orthogonal milling of CFRP laminates. Compos Part B Eng 109:10–22. https://doi.org/10.1016/j.compositesb.2016.10.015
22. Karpat Y, Bahtiyar O, Değer B (2012) Mechanistic force modeling for milling of unidirectional carbon fiber reinforced polymer laminates. Int J Mach Tools Manuf 56:79–93. https://doi.org/10.1016/j.ijmachtools.2012.01.001
23. Qi Z, Zhang K, Cheng H et al (2015) Microscopic mechanism based force prediction in orthogonal cutting of unidirectional CFRP. Int J Adv Manuf Technol 79:1209–1219. https://doi.org/10.1007/s00170-015-6895-7
24. Su Y, Jia Z, Niu B, Bi G (2017) Size effect of depth of cut on chip formation mechanism in machining of CFRP. Compos Struct 164:316–327. https://doi.org/10.1016/j.compstruct.2016.11.044
25. Kim D-G, Yang S-H (2023) Efficient Analysis of CFRP Cutting Force and Chip Formation Based on Cutting Force Models Under Various Cutting Conditions. Int J Precis Eng Manuf 24:1235–1251. https://doi.org/10.1007/s12541-023-00822-7
26. Biró I, Szalay T (2017) Extension of empirical specific cutting force model for the process of fine chip-removing milling. Int J Adv Manuf Technol 88:2735–2743. https://doi.org/10.1007/s00170-016-8957-x
27. Balázs BZ, Takács M (2018) Finite element modelling of thin chip removal process. IOP Conf Ser Mater Sci Eng 426:012002. https://doi.org/10.1088/1757-899X/426/1/012002
28. Zhang P, Wang C, Ying Z, Sugita N (2026) Improved cutting mechanism and surface generation of CFRP with ultrasonic vibration. Precis Eng 99:440–452. https://doi.org/10.1016/j.precisioneng.2026.01.031
29. Hintze W, Hartmann D, Schütte C (2011) Occurrence and propagation of delamination during the machining of carbon fibre reinforced plastics (CFRPs) – An experimental study. Compos Sci Technol 71:1719–1726. https://doi.org/10.1016/j.compscitech.2011.08.002
30. Böhland F, Hilligardt A, Schulze V (2024) Analysis of subsurface damage during milling of CFRP due to spatial fibre cutting angle, tool geometry and cutting parameters. Compos Part B Eng 281:111533. https://doi.org/10.1016/j.compositesb.2024.111533
31. Li J, Xu K, Lin Z, Fu J (2024) A unified geometrical modeling and analysis method for evaluating CFRP machining performance: Cutting geometry space. Compos Part B Eng 283:111649. https://doi.org/10.1016/j.compositesb.2024.111649
32. Geier N, Pereszlai C (2020) Analysis of Characteristics of Surface Roughness of Machined CFRP Composites. Period Polytech Mech Eng 64:67–80. https://doi.org/10.3311/PPme.14436
33. Turki Y, Habak M, Velasco R, Vantomme P (2017) Highlighting cutting mechanisms encountered in carbon/epoxy composite drilling using orthogonal cutting. Int J Adv Manuf Technol 92:685–697. https://doi.org/10.1007/s00170-017-0153-0
34. Yazman Ş, Gemi L, Morkavuk S, Köklü U (2024) Investigation of the effect of symmetrical hybrid stacking on drilling machinability of unidirectional CFRP, GFRP and hybrid composites: Drilling tests and damage analysis. Compos Part Appl Sci Manuf 187:108486. https://doi.org/10.1016/j.compositesa.2024.108486
35. Doğan MA, Yapici A, Gemi L et al (2025) Investigation of the stacking sequence and cutting parameters effect on hole morphology in hybrid FML composites. Compos Part B Eng 300:112464. https://doi.org/10.1016/j.compositesb.2025.112464
36. Yazman Ş (2021) The effects of back-up on drilling machinability of filament wound GFRP composite pipes: Mechanical characterization and drilling tests. J Manuf Process 68:1535–1552. https://doi.org/10.1016/j.jmapro.2021.06.054
37. Gemi L, Morkavuk S, Köklü U, Yazman Ş (2020) The effects of stacking sequence on drilling machinability of filament wound hybrid composite pipes: Part-2 damage analysis and surface quality. Compos Struct 235:111737. https://doi.org/10.1016/j.compstruct.2019.111737
38. Erhan F, Gemi L, Yazman Ş et al (2025) A comprehensive investigation into the influence of variation in the stacking sequence on the mechanical behaviour and drilling machinability of basalt fiber-reinforced composite tubes. Compos Part B Eng 299:112405. https://doi.org/10.1016/j.compositesb.2025.112405
39. Li HN, Wang JP, Wu CQ et al (2020) Damage behaviors of unidirectional CFRP in orthogonal cutting: A comparison between single- and multiple-pass strategies. Compos Part B Eng 185:107774. https://doi.org/10.1016/j.compositesb.2020.107774
40. Han L, Zhang J, Wang H (2023) Mediating compositional machining difference of UD-CFRP in orthogonal cutting by epoxy coating. Compos Part B Eng 258:110706. https://doi.org/10.1016/j.compositesb.2023.110706
41. Vallejo J, García-Plaza E, Núñez PJ et al (2023) Machinability analysis of carbon fibre reinforced PET-Glycol composites processed by additive manufacturing. Compos Part Appl Sci Manuf 172:107561. https://doi.org/10.1016/j.compositesa.2023.107561
42. Qin X, Gao Y, Kang P et al (2024) Research on the influence of cutting thickness on CFRP material removal behavior considering tool wear. J Mater Res Technol 29:4018–4035. https://doi.org/10.1016/j.jmrt.2024.02.128
43. Riaz A, Yuan Z, Chohan BS, Cheng K (2025) Experimental study on the influence of blade shape-composite interaction for dicing CFRP composites. Int J Adv Manuf Technol 140:1317–1333. https://doi.org/10.1007/s00170-025-16285-1
44. Geier N, Szalay T, Takács M (2018) Analysis of thrust force and characteristics of uncut fibres at non-conventional oriented drilling of unidirectional carbon fibre-reinforced plastic (UD-CFRP) composite laminates. Int J Adv Manuf Technol 100:3139–3154. https://doi.org/10.1007/s00170-018-2895-8
45. Geier N, Szalay T (2017) Optimisation of process parameters for the orbital and conventional drilling of uni-directional carbon fibre-reinforced polymers (UD-CFRP). Measurement 110:319–334. https://doi.org/10.1016/j.measurement.2017.07.007
46. Ahmad J (2009) Machining of Polymer Composites. Springer US, Boston, MA
47. An Q, Ming W, Cai X, Chen M (2015) Study on the cutting mechanics characteristics of high-strength UD-CFRP laminates based on orthogonal cutting method. Compos Struct 131:374–383. https://doi.org/10.1016/j.compstruct.2015.05.035
48. Gara S, Tsoumarev O (2016) Prediction of surface roughness in slotting of CFRP. Measurement 91:414–420. https://doi.org/10.1016/j.measurement.2016.05.016
49. Fiber pull-out damage formations and their effect on hole quality when drilling carbon fiber reinforced plastic (CFRP) composites using various tool geometries | Journal of Mechanical Science and Technology. https://link.springer.com/article/https://doi.org/10.1007/s12206-023-0743-8. Accessed 1 Sept 2025
50. Ashworth S, Fairclough JPA, Sharman ARC et al (2019) Varying CFRP workpiece temperature during slotting: Effects on surface metrics, cutting forces and chip geometry. Procedia CIRP 85:37–42. https://doi.org/10.1016/j.procir.2019.09.021

51. Morkavuk S, Köklü U, Bağcı M, Gemi L (2018) Cryogenic machining of carbon fiber reinforced plastic (CFRP) composites and the effects of cryogenic treatment on tensile properties: A comparative study. Compos Part B Eng 147:1–11. https://doi.org/10.1016/j.compositesb.2018.04.024
52. Microscopic mechanism based force prediction in orthogonal cutting of unidirectional CFRP | The International Journal of Advanced Manufacturing Technology https://link.springer.com/article/https://doi.org/10.1007/s00170-015-6895-7. Accessed 1 Sept 2025
53. Ashworth S, Fairclough JPA, Takikawa Y et al (2019) Effects of machine stiffness and cutting tool design on the surface quality and flexural strength of edge trimmed carbon fibre reinforced polymers. Compos Part Appl Sci Manuf 119:88–100. https://doi.org/10.1016/j.compositesa.2019.01.019
54. Madhavan V, Lipczynski G, Lane B, Whitenton E (2015) Fiber orientation angle effects in machining of unidirectional CFRP laminated composites. J Manuf Process 20:431–442. https://doi.org/10.1016/j.jmapro.2014.06.001
55. Efficient Analysis of CFRP Cutting Force and Chip Formation Based on Cutting Force Models Under Various Cutting Conditions | International Journal of Precision Engineering and Manufacturing. https://link.springer.com/article/https://doi.org/10.1007/s12541-023-00822-7. Accessed 1 Sept 2025